The H19/let-7 double-negative feedback loop contributes to glucose metabolism in muscle cells

Yuan Gao, Fuju Wu, Jichun Zhou, Lei Yan, Michael Jurczak, Hui-Young Lee, Lihua Yang, Martin Mueller, Xiao-Bo Zhou, Luisa Dandolo, et al.

Nucleic Acids Research Advance Access published November 15, 2014

Nucleic Acids Research, 2014 **1**
doi: 10.1093/nar/gku1160

The H19/let-7 double-negative feedback loop contributes to glucose metabolism in muscle cells

Yuan Gao[1,2,†], Fuju Wu[1,3,†], Jichun Zhou[1,4], Lei Yan[1,5], Michael J. Jurczak[6], Hui-Young Lee[6], Lihua Yang[1,7], Martin Mueller[1,8], Xiao-Bo Zhou[1,9], Luisa Dandolo[10], Julia Szendroedi[11,12], Michael Roden[11,12], Clare Flannery[1], Hugh Taylor[1], Gordon G. Carmichael[13], Gerald I. Shulman[6] and Yingqun Huang[1,*]

[1]Department of Obstetrics, Gynecology and Reproductive Sciences, Yale Stem Cell Center, Yale University School of Medicine, New Haven, CT 06510, USA, [2]Department of Gynecology and Obstetrics, Chinese PLA General Hospital, Beijing 100853, P. R. China, [3]Department of Obstetrics and Gynecology, Jilin University, Changchun, Jilin 130021, P. R. China, [4]Department of Surgical Oncology, Affiliated Sir Run Run Shaw Hospital, Zhejiang University School of Medicine, Hangzhou, Zhejiang 310016, P. R. China, [5]Department of Obstetrics and Gynecology, Shandong Provincial Hospital Affiliated to Shandong University, Jinan, Shandong 250021, P. R. China, [6]Howard Hughes Medical Institute and Departments of Internal Medicine, Cellular & Molecular Physiology, Yale University School of Medicine, New Haven, CT 06510, USA, [7]Obstetrics and Gynecology Department, Tangshan Gongren Hospital, Tangshan, Hebei 063000, P. R. China, [8]Department of Obstetrics and Gynecology, University Hospital, 3012 Bern, Switzerland, [9]Department of Immunology and Pathogenic Biology, School of Medicine, Xi'an Jiaotong University, Xi'an, Shaanxi 710061, P. R. China, [10]Department of Genetics and Development, Institut Cochin, U1016 Paris, France, [11]Institute for Clinical Diabetology, German Diabetes Center, Leibniz Center for Diabetes Research, 40225 Dusseldorf, Germany, [12] Department of Metabolic Diseases, Heinrich Heine University, 40225 Dusseldorf, Germany and [13]Department of Genetics and Developmental Biology, University of Connecticut Health Center, Farmington, CT 06030, USA

Received September 9, 2014; Revised October 15, 2014; Accepted October 29, 2014

ABSTRACT

The H19 lncRNA has been implicated in development and growth control and is associated with human genetic disorders and cancer. Acting as a molecular sponge, H19 inhibits microRNA (miRNA) let-7. Here we report that H19 is significantly decreased in muscle of human subjects with type-2 diabetes and insulin resistant rodents. This decrease leads to increased bioavailability of let-7, causing diminished expression of let-7 targets, which is recapitulated *in vitro* where H19 depletion results in impaired insulin signaling and decreased glucose uptake. Furthermore, acute hyperinsulinemia down-regulates H19, a phenomenon that occurs through PI3K/AKT-dependent phosphorylation of the miRNA processing factor KSRP, which promotes biogenesis of let-7 and its mediated H19 destabilization. Our results reveal a previously undescribed double-negative feedback loop between sponge lncRNA and target miRNA that contributes to glucose regulation in muscle cells.

INTRODUCTION

The H19 long noncoding RNA (lncRNA) is transcribed from a conserved imprinted gene cluster that also contains the nearby *Igf2* gene encoding insulin-like growth factor 2 (1). The two genes are reciprocally imprinted, with *H19* being maternally and *Igf2* paternally expressed. Both genes are highly expressed during fetal life and are strongly down-regulated after birth, except for persistent expression of *H19* in adult skeletal muscle and heart. *H19* encodes a 2.6 kb capped, spliced and polyadenylated noncoding RNA that is predominantly cytoplasmic, with a minor fraction also found in the nucleus (1). Important for embryo development and growth control, the *H19-Igf2* locus has been implicated in two human genetic disorders: Beckwith–Wiedemann Syndrome (BWS) and Silver–Russell Syndrome (SRS). BWS is also associated with a predisposition to tumorigenesis (1). Evidence supports a growth-suppressing role of *H19* (2), although an oncogenic role cannot be ruled out (3–6). Nuclear H19 binds EZH2 (a key component of Polycomb repressive complex 2) and inhibits transcription of a selective group of genes, thereby promoting bladder cancer metastasis (4). Likewise, through interaction with MBD1 (methyl-CpG-binding protein 1)

*To whom correspondence should be addressed. Tel: +1 203 737 2578; Fax: +1 203 785 7134; Email: yingqun.huang@yale.edu
†The authors wish it to be known that, in theiropinion, the first two authors should be regarded as Joint First Authors.

nuclear H19 inhibits expression of imprinted network genes by recruiting repressive histone markers to their differentially methylated regions, contributing to embryo growth regulation (7). In addition to epigenetic modification, the nuclear role of H19 extends to its ability to encode miR-675, a microRNA (miRNA) embedded in its first exon and whose release from H19 is developmentally tightly controlled in the mouse (8,9). miR-675 functions to both regulate placental growth and maintain adult hematopoietic stem cells, in part by post-transcriptionally inhibiting *Igfr1* expression (9,10). Further, it acts to promote skeletal muscle differentiation and regeneration (11).

Consistent with its predominantly cytoplasmic localization, H19 has recently been shown to act as a molecular 'sponge' to sequester and regulate the let-7 family miRNAs (12). While noncoding RNAs as miRNA sponges regulating miRNA functions have been increasingly described (12–20), whether these molecules are recriprocally regulated by their target miRNAs, and how such regulation may occur, remain unclear.

It has been reported that transgenic mice with inducible muscle-specific overexpression of let-7 display insulin resistance and impaired glucose tolerance, a phenotype that occurs in part through let-7-mediated repression of multiple components of the insulin-PI3K-mTOR pathway, including insulin receptor (Insr), insulin receptor substrate 2 (Irs2) and insulin-like growth factor receptor 1 (Igfr1) (21). Likewise, global let-7 overexpression in transgenic mice leads to impaired glucose tolerance, whereas anti-miR-induced let-7 downregulation both prevents and treats high fat diet (HFD)-induced glucose intolerance, due at least in part to improved insulin signaling as a result of derepression of let-7 targets Insr and Irs2 in the muscle and liver (22). Thus, genetic manipulation of let-7 level can cause altered glucose metabolism (21,22). However, therein lies a paradox: neither HFD mice (22) nor mice with muscle-specific Lin28 knockout (21) exhibited increased levels of let-7 in their skeletal muscle, despite the fact that these mice were diabetic (21,22). Since Lin28 is a developmentally regulated RNA-binding protein that functions to block processing of primary let-7 transcripts (pri-let-7) to mature let-7 (23–25), one would predict that muscle-specific Lin28 knockout mice would have increased levels of let-7, but in fact this is not the case (21). This raises the intriguing possibility that some other factor, rather than Lin28, might regulate let-7 in muscle.

In this report we demonstrate that H19 acts as an upstream regulator of let-7 in skeletal muscle cells; it reduces the bioavailability of let-7 without altering its expression level. Also, we reveal that there exists a double-negative regulatory feedback loop between let-7 and H19 that may underlie glucose regulation in muscle cells.

MATERIALS AND METHODS

Antibodies, siRNAs, miRNAs and inhibitors

Antibodies for INSRβ (rabbit polyclonal, Bethyl Laboratories, Inc., A303–712A), Lipoprotein lipase (LPL) (mouse monoclonal, Abcam, ab21356), β-tubulin (rabbit polyclonal, Abcam, ab6046), Protein kinase B (AKT) (rabbit polyclonal, Cell Signalling Technology, 9272), phospho-AKT (Ser473) (rabbit polyclonal, Cell Signalling Technology, 9271), S6 ribosomal protein (rabbit monoclonal, Cell Signalling Technology, 2217), phospho-S6 ribosomal protein (Ser235/236) (rabbit monoclonal, Cell Signalling Technology, 4856) and KH domain-containing AU-rich element(ARE) binding protein (KSRP) (rabbit polyclonal, Cell Signalling Technology, 2217) were purchased. Inhibitors specific for AKT (124005 Akt inhibitor, Calbiochem, 124005) and PI3K (LY294002, Selleckchem, S1105) were purchased. The AKT and PI3K inhibitors were prepared in Dimethyl sulfoxide (DMSO) with stock concentrations of 10 and 30 mM, respectively, and diluted in culture medium at 1:1000 to obtain working concentrations of 10 and 30 μM, respectively.

Mouse H19-specific siRNA (simH19, 4390815/n25 3566), let-7a miRNA (AM17100/PM10050), miR16–1 miRNA (AM17100/PM10339), miR negative control (miCon, AM17110), let-7 inhibitor (iLet-7, 4392431) and anti-miR control (iCon, AM17010) were previously described (12). The miR-16 inhibitor (imiR-16, 4464084) and siKSRP targeting the mouse KSRP coding region (5′-CAGGACAGUUUCACGACAACG-3′ (26–28)) were purchased from Ambion.

Plasmids

psiCHECK2-let-7 4x was previously described (12). To make psiCHECK2-LPL, polymerase chain reaction (PCR) was carried out using adult mouse muscle cDNA as a template and forward 5′-ccgctcgagAGCTTGTAATTGAGGTGACA and reverse 5′-aaggaaaaaagcggccgcCAGGAAGCTAAGGCAGGATG primers. The resulting 190-bp mouse LPL (accession number BC003305) fragment was cloned to psiCHECK2-let-7 4x opened with XhoI and NotI. To make psiCHECK2-LPLmt, PCR was carried out using psiCHECK2-LPL as a template and forward 5′-ccgctcgagAGCTTGTAATTGAGGTGACA and reverse 5′-aaggaaaaaagcggccgcCAGGAAGCGAACTCACGATG primers. The resulting 190-bp mouse LPL fragment with point mutations was cloned to psiCHECK2-let-7 4x opened with XhoI and NotI. The clones were verified by sequencing.

Mouse muscle samples

Male C57BL/6 mice were maintained at 24°C on a 12-h:12-h light-dark cycle. Mice were fed a regular chow (Harlan Teklad 2018S) or HFD (60% kcal fat; Research Diets, D12492) for seven weeks. Animals were fasted overnight for 14 h before sampling. Mice were euthanized by cervical dislocation after anesthesia with isoflurane, and quadriceps muscle was rapidly isolated and snap-frozen with precooled aluminum forceps and liquid nitrogen prior to storage at −80°C. All experiments were performed in accordance with Yale's Institutional Animal Care and Use Committee regulations.

Human muscle samples

The study was approved by the local ethics committee in accordance with the most recent version of the Helsinki Declaration. Written consent was obtained from each subject after the purpose, nature and potential complications of the studies had been explained. During muscle biopsy, the skin over the lateral quadriceps muscle was sterilely prepared with betadine, and 1% lidocaine was injected subcutaneously. A 2-cm incision was made using a scalpel and a baseline punch muscle biopsy was extracted using a 5-mm Bergstrom biopsy needle. A piece of muscle tissue was dissected with scalpel and immediately blotted, snap frozen and stored in liquid nitrogen until use. The characteristics of the subjects (four healthy lean and five type-2 diabetes (T2D)) are shown in the Supplementary Table S1.

Hyperinsulinemia/euglycemic clamp experiments

Twelve- to fourteen-week old male C57BL6/J mice maintained on regular chow (Harlan Teklad 2018S) underwent surgery to implant indwelling catheters in the left jugular vein. One week after surgery, mice were fasted overnight and either euthanized with intravenous pentobarbital for basal tissue or infused with 3 mU/kg/min insulin and 20% dextrose to maintain euglycemia (∼120 mg/dl) for 140 min. Plasma insulin levels were 45.8 −/+ 3.2 uU/ml at the end of the experiment. Mice were euthanized, and gastrocnemius and quadriceps muscle were rapidly isolated and snap-frozen with pre-cooled aluminum forceps and liquid nitrogen prior to storage at −80°C. All experiments were performed in accordance with Yale's Institutional Animal Care and Use Committee regulations.

Mouse C3H muscle myoblast culture and differentiation

Low passage C3H myoblast line was derived from normal adult C3H mouse leg muscle (Sigma-Aldrich, 91031101-1VL). Undifferentiated C3H myoblasts were maintained in growth medium (GM) (Dulbecco's modifiedEagle's medium (DMEM), Gibco, catalog number 11965-092, supplemented with 10% Fetal Bovine Serum (FBS), heat inactivated, 1% penicillin/streptomycin, 1% L-glutamine and 1-mM sodium pyruvate). To prepare for differentiation, cells were typically seeded in 6-well plates at a density of 2.0×10^5 cells/well in GM. Differentiation was initiated 2 days later by replacing medium with differentiation medium (DM) (DM containing 2% horse serum in place of 10% FBS). The medium was partially changed every other day until use.

C3H myotube transfection

Transfection was performed at day 3 or 4 after initiation of differentiation. Mytotubes were washed once with pre-warmed OPTI-Minimal Essential Medium (OPTI-MEM) immediately before addition of transfection cocktails. To prepare transfection cocktails for each well of 6-well plates, 500-pmol of siCon or siH19 (with a stock solution of 5 μM) was mixed with 600 μl of OPTI-MEM by gentle pipetting. In parallel 25 μl of Lipofectamine 2000 was diluted in 600 μl of OPTI-MEM by gentle pipetting. After 5 min incubation at room temperature (RT), the two were combined by gentle pipetting. Following incubation at RT for 20 min, the resulting cocktail (1200 μl) was applied to myotubes that were pre-washed with OPTI-MEM. After overnight incubation in a tissue culture incubator, the cocktail was replaced with fresh DM. Forty-eight hours later, RNA and protein were extracted for analysis.

For miRNA transfection, 32 pmol of miCon or let-7a, or 16 pmol of iCon or iLet-7 (with a stock concentration of 5 μM) was mixed with 400 μl of OPTI-MEM by gentle pipetting. In parallel, 4 μl of Lipofectamine 2000 was mixed with 400 μl of OPTI-MEM. Following 5 min of RT incubation, the two solutions were mixed and incubated at RT for 20 min. The resulting 800 μl of transfection cocktail was directly applied to one well of mytotubes pre-washed with OPTI-MEM. After overnight incubation, the cocktail was replaced with fresh DM. RNA and protein were extracted 48 h post-transfection for analysis.

Glucose uptake assay

These were performed in a 96-well plate scale. Glucose uptake assays were carried out using the Glucose Uptake Cell-Based Assay Kit (Cayman Chemical, catalog number 600470) according to the manufacturer's instructions with minor modifications. Briefly, 48 h after siRNA transfection, myotubes were incubated in 200 μl of glucose-free DMEM (Gibco, catalog number 11966–025) in the presence or absence of 100 nM of insulin for 2 h. The medium was then removed and replaced with 100 μl of new glucose-free DMEM containing fluorescent 2-NBDG at a final concentration of 150 μg/ml. Incubation was carried out in dark for an additional 10 min in the tissue culture incubator. The medium was then removed and the cells washed once with 200 μl of ice-cold phosphate buffered saline (PBS). After adding 100 μl of new ice-cold PBS to the cells, fluorescent intensity was immediately determined using the fluorescent plate reader (FilterMax F3&F5 Multi-Mode Microplate Reader, Molecular Devices).

RNA stability analysis

To assess insulin effects on H19 RNA stability, C3H myotubes in 48-well plates were incubated with 100 nM of insulin (HUMULIN R, Lilly USA, LLC, Indianapolis) in DM in the presence of actinomycin D at a final concentration of 10 ug/ml for a total duration of 1.5 h. Total RNA was harvested at 0, 30, 60 and 90 min and analyzed by RT-qPCR. Results are presented after normalization against beta-tubulin mRNA levels with 0 time point RNA levels arbitrarily set as 1.

To evaluate let-7 effects on H19 RNA stability, miRNA transfection (48-well plate scale) combined with actinomycin D time course analysis was performed. To prepare transfection cocktail, 1 pmol of miCon or let-7a was mixed with 50 μl of OPTI-MEM. In parallel, 0.5 μl of Lipofectamine 2000 was mixed with 50 μl of OPTI-MEM. Following 5 min of incubation, the two solutions were mixed and incubated at RT for 20 min. The resulting 100 μl of transfection cocktail was added to myotubes pre-washed with OPTI-MEM. Upon adding the transfection cocktail, acti-

nomycin D was also added to each well at a final concentration of 10 μg/ml. Total RNA was extracted at 0, 1, 2 and 3 h, followed by RT-qPCR analysis. Results are presented after normalization against beta-tubulin mRNA levels with 0 time point RNA levels arbitrarily set as 1.

PI3K/AKT inhibitor rescue experiments

These were performed in a 48-well plate scale. Day 3 myotubes were incubated with fresh 200 μl of DM containing 30 μM of PI3K inhibitor (group #1), 10 μM of AKT inhibitor (group #2) or no inhibitors (groups #3 and #4). After 30 min incubation, 200 μl of new DM containing 30 μM of PI3K inhibitor plus 200 nM of Insulin (INS) was added to group #1; 200 μl of new DM containing 10 μM of AKT inhibitor plus 200 nM of INS was added to group #2; 200 μl of new DM containing 200 nM of INS was added to group #3; and 200 μl of new DM containing no inhibitors or INS was added to group #4. Thus, the #1 and #2 groups were exposed to both INS (at a final concentration of 100 nM) and the respective inhibitors. The #3 group was exposed to INS only, while the #4 group was exposed to none. Medium was not removed at the end of 30 min pre-incubation to avoid cell detachment. After 2 h, medium was removed and cells in these four wells were lysed with Lysis Butter. Following regular RNA extraction, reverse transcription and RT-qPCR was performed as described below.

RT-qPCR analysis

These were carried out essentially as previously described (12). Briefly, total RNAs were extracted from cells using PureLink RNA Mini Kit (Ambion, catalog number 12183018A). cDNA was synthesized using Bio-Rad iSCRIPT kit (1725122) in a 20-μl reaction containing 100–500 ng of total RNA. Real-time quantitative PCR was performed in a 15-μl reaction containing 0.5–1 μl of cDNA using iQSYBRGreen (Bio-Rad) in a Bio-Rad iCycler. PCR was performed by initial denaturation at 95°C for 5 min, followed by 40 cycles of 30 s at 95°C, 30 s at 60°C and 30 s at 72°C. Specificity was verified by melting curve analysis and agarose gel electrophoresis. The threshold cycle (Ct) values of each sample were used in the post-PCR data analysis. The PCR primers for the indicated human, mouse and rat genes are listed below.

Human H19 forward: 5′- ACTCAGGAATCGGCTCTGGAA
Human H19 reverse: 5′- CTGCTGTTCCGATGGTGTCTT
Mouse H19 forward: 5′-CCTCAAGATGAAAGAAATGGTGCTA
Mouse H19 reverse: 5′-TCAGAACGAGACGGACTTAAAGAA
Rat H19 forward: 5′-ACTCCATCTTCATGGCCAAC
Rat H19 reverse: 5′-CAGAGTCACGGATGCTTTGA
Mouse Lpl forward: 5′-GGATCCGTGGCCGCAGCAGACGCAGGAAGA
Mouse Lpl reverse: 5′-GAATTCCATCCAGTTGATGAATCTGGCCAC
Mouse Igf2 forward: 5′-GCTTGTTGACACGCTTCAGTTTG
Mouse Igf2 reverse: 5′-GTTGGCACGGCTTGAAGGC
Mouse INSRβ forward: 5′-GCTGGAGGAGTCTTCATTCA
Mouse INSRβ reverse: 5′-TGCCTGAAGAGGTTTTTCTG
Human/mouse beta-tubulin forward: 5′-CGTGTTCGGCCAGAGTGGTGC
Human/mouse beta-tubulin reverse: 5′-GGGTGAGGGCATGACGCTGAA
Rat/mouse RPLP0 (36B4) forward: 5′-AGATGCAGCAGATCCGCAT
Rat/mouse RPLP0 (36B4) reverse: 5′-GTTCTTGCCCATCAGCACC

For miRNA quantification, total RNAs were extracted from cells using PureLink RNA Mini Kit (Ambion, catalog number 12183018A). Levels of mature miRNAs were determined by RT-qPCR using miScript reverse transcription kit (catalog number 218161) and miScript SYBR Green PCR kit (catalog number 218073) according to the manufacturers' instructions. PCR primer sets (miScript primer) specific for let-7a (MS00031220), miR16–1 (MS00006517), miR-1 (MS00008358), miR-133 (MS00032305), miR-675 (MS00006398) and snRNA U6 (MS00033740) were purchased from Qiagen. The indicated miRNA levels were normalized against U6.

Western blot analysis

These were carried out essentially as previously described (12). Briefly, cell or frozen tissue pellets were quickly lysed in five volumes of 2x sodium dodecyl sulphate (SDS)-sample buffer heated at 100°C for 5 min, with occasional vortexing. Five to ten microliters of homogenized samples were loaded onto 10% SDS gel, followed by western blot analysis.

Luciferase assays

The assays were carried out in a 48-well plate scale as previously described (12). Briefly, 10 ng of the indicated luciferase reporter plus 140 ng of empty vector was transfected into HEK293 cells (2×10^5 cell/well), together with control miRNA or let-7 miRNAs at a final concentration of 24, 48 or 96 nM. Each concentration was run in triplicates. Luciferase activities were measured 18 h post-transfection using Promega Dual-Luciferase Reporter Assay System (E1960) according to the manufacturer's protocol. Renilla luciferase activities were normalized against Firefly luciferase activities and presented as percentage of inhibition.

Bioinformatic analysis

The sequences of human and mouse lipoprotein lipase (Lpl) genes were retrieved from Genebank (http://www.ncbi.nlm.nih.gov/gene) using their corresponding accession numbers of BC011353.1 and BC003305, respectively. The sequences of human and mouse mature miRNAs were retrieved from miRBase (http://www.mirbase.org/). The binding sites of let-7 miRNA on Lpl mRNAs were predicted using a web-based program RNAhybrid (12).

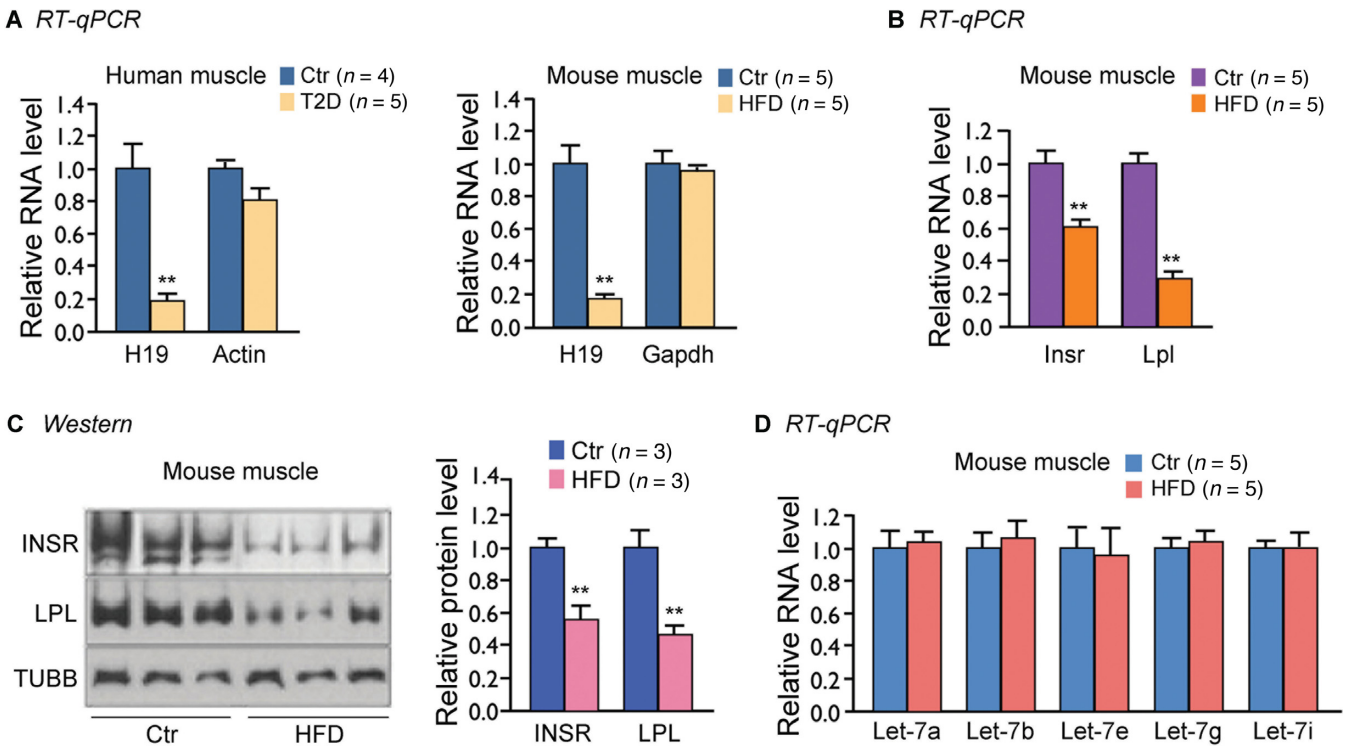

Figure 1. H19 is downregulated in skeletal muscle of diabetic human subjects and high fat diet (HFD) induced insulin resistant and diabetic mice. (**A**) Relative H19 expression in non-diabetic (Ctr) versus T2D human/HFD mouse muscle. Numbers of mice and human subjects are indicated in the parenthesis. (**B**) Relative Insr and Lpl mRNA levels in Ctr versus HFD mouse muscle. (**C**) Protein lysates from muscle of Ctr or HFD mice were used to analyze expression levels of Insr and Lpl by western blot analysis. Beta-tubulin (TUBB) was used as a loading control. Quantifications of the western blot bands are shown on the right. (**D**) Relative let-7 levels in Ctr versus HFD mouse muscle. All data are presented as mean ± SEM. $^{*}P < 0.05$; $^{**}P < 0.01$.

Statistical analysis

All data are presented as mean ± SEM. Data were analyzed using two-tailed Student's *t*-test. *P*-values of 0.05 or less were considered significant.

RESULTS

Decreased H19 expression correlates with impaired glucose homeostasis in human and mouse

Both human and mouse skeletal muscle express high levels of H19 (1,29). Intriguingly, we observed that the H19 level was ∼5-fold downregulated in muscle of both human subjects with T2D and insulin resistant mice, as compared to healthy controls (Figure 1A). HFD-induced obesity is a well-characterized mouse model of obesity-induced insulin resistance and T2D (22). We previously identified three let-7-binding sites in mouse H19 (Supplementary Figure S1, (12)). Given that H19 sequesters let-7, preventing it from inhibiting target gene expression (12), we hypothesized that decreased levels of H19 would lead to less sequestration of let-7, causing more let-7 to be available to inhibit target gene expression, hence contributing to and exacerbating insulin resistance and T2D. To test the hypothesis, we examined expression of two let-7 targets, Insr and Lpl. The Insr (composed of two extracellular α-subunits linked to a transmembrane-spanning β-subunit) is responsible for insulin action in peripheral tissues including liver, fat and skeletal muscle and is a key player in the evolutionarily conserved insulin-PI3K-mTOR signaling pathway that regulates growth and glucose metabolism (21,22,30). The *Insr* genes of both human and mouse contain a single let-7-binding site in their 3′-UTRs (21,22). The lipoprotein lipase is most widely distributed in adipose, heart and skeletal muscle tissue. It hydrolyzes triglycerides in lipoproteins into fatty acids and monoacylglycerol molecules for tissue utilization and also promotes cellular uptake of free fatty acids, cholesterol-rich lipoproteins and chrylomicron remnants (31). In addition to its central role in lipid metabolism, lipoprotein lipase has a function of regulating mitochondrial biogenesis. Indeed, decreased lipoprotein lipase level contributes to reduced mitochondrial number, and down-regulation of *Lpl* and mitochondrial number in muscle of young lean insulin resistant offspring of parents with T2D have been documented (32). Based on a strong relationship between diminished mitochondrial number and muscle insulin resistance (33–35), a role of lipoprotein lipase in glucose metabolism has been proposed (32).

We identified let-7-binding sites in the 3′-UTR of Lpl mRNA of both human (position 2143) and mouse (position 2940) (Supplementary Figure S2). Importantly, the expressions of *Insr* and *Lpl* were significantly decreased at both RNA (Figure 1B) and protein (Figure 1C) levels in HFD muscle compared to normal controls. Consistent with previous reports (22), there was no significant difference in the let-7 level between the two groups (Figure 1D). These results suggested that downregulation of H19 increased the bioavailability of let-7 without affecting its level, leading to

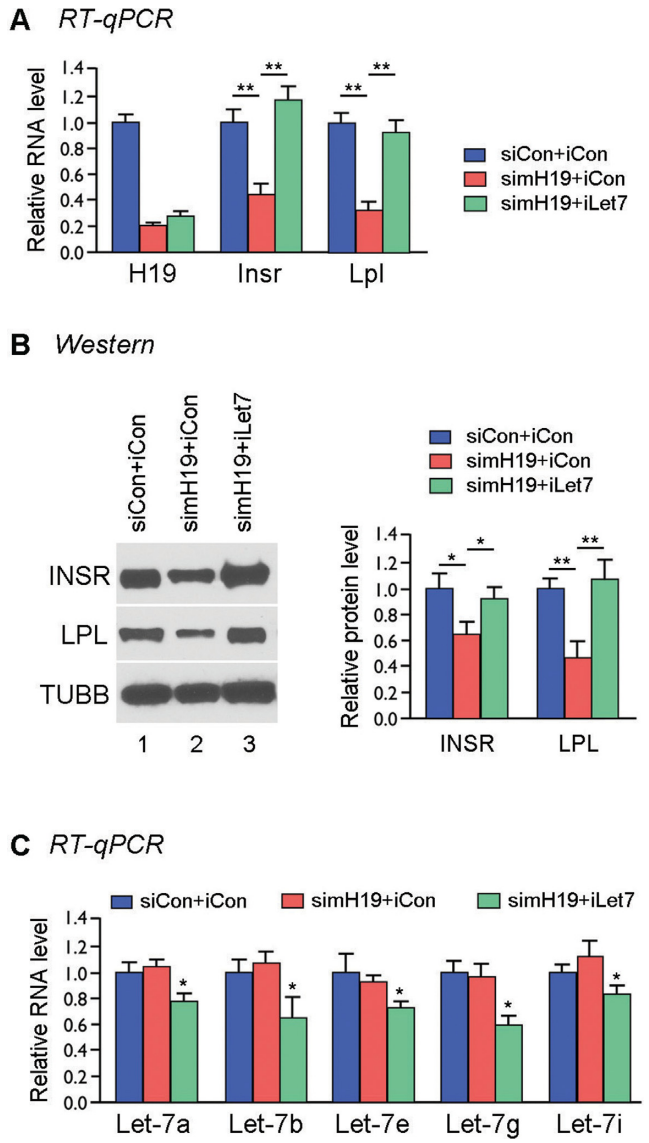

Figure 2. The H19/let-7 axis regulates expression of insulin receptor and lipoprotein lipase. C3H myotubes were transfected with the indicated mixture. Protein and RNA were extracted 48 h later and levels determined by RT-qPCR (**A** and **C**) and western blot (**B**) analyses. In (B), quantification of western gels from three independent experiments are shown on the right. All data are presented as mean ± SEM. ($n = 3$); $^{*}P < 0.05$; $^{**}P < 0.01$.

decreased expression of *Insr* and *Lpl*. Further, while H19 was diminished in the HFD muscle (Supplementary Figure S3A), the levels of miR-675 and Igf2 were not significantly altered (Figure S3B and C), suggesting that miR-675 and Igf2 were likely not associated with the HFD effects.

To provide further evidence that the decreased expression of *Insr* and *Lpl* was indeed mediated by let-7, we performed siRNA knockdown combined with let-7 inhibition experiments in myotubes differentiated from mouse C3H myoblasts. The specific questions we asked were whether H19 knockdown would reduce the expression of *Insr* and *Lpl* and whether co-transfection of a let-7-specific inhibitor (iLet7) concomitant with H19 knockdown would reverse this effect. iLet7 is a chemically-modified, single-stranded nucleic acid that specifically binds to and inhibits endogenous let-7 molecules (12). Thus, C3H myotubes were transfected with a mix of siCon (control siRNA) and iCon (control miRNA inhibitor), a mix of simH19 (a siRNA specific for mouse H19, (12)) and iCon or a mix of simH19 and iLet7. Protein and RNA were extracted and analyzed 48 h post-transfection. Results from control experiments using siCon, simH19, iCon or iLet7 alone are also shown (Supplementary Figure S4). When H19 was knocked down by ∼80% (Figure 2A, left column, compare red bar to blue bar), the mRNA levels of both *Insr* and *Lpl* were reduced significantly (middle and right columns, compare red bars to blue bars). In contrast, when H19 was knocked down (left column, compare green bar to blue bar) but at the same time iLet7 was also present, a decrease in the Insr and Lpl mRNA levels was not observed (middle and right columns, compare green bars to blue bars). The changes in *Insr* and *Lpl* expression at the protein level in response to H19 knockdown and iLet7 rescue were consistent with those of mRNA levels (Figure 2B). Together, these results suggested that the effects of H19 knockdown on *Insr* and *Lpl* expression were indeed mediated by let-7. While H19 depletion did not affect let-7 levels (Figure 2C, compare red bars to blue bars across the columns), co-transfection with iLet7 led to modest decreases in let-7 levels (compare green bars to blue bars), consistent with targeted let-7 degradation by antisense inhibitors (22). Collectively, our results further underscore the notion that H19 facilitates expression of *Insr* and *Lpl* in muscle cells by reducing the bioavailability of let-7.

H19 depletion impairs insulin sensitivity of muscle cells

A hallmark of heightened glucose metabolism is an increase in glucose uptake, which can be assessed quantitatively using well-established methods involving radioactive or non-radioactive glucose tracers. To assess the biological significance of H19 in glucose metabolism, we analyzed effects of H19 downregulation on insulin-stimulated glucose uptake in C3H myotubes. We used a non-radioactive glucose uptake method that employs 2-NBDG, a fluorescently-labeled deoxyglucose analog, as a tracer for direct monitoring of glucose transport in live cells. Thus, siCon or simH19 was transfected into myotubes, followed by glucose uptake assays 48 h post transfection. As expected, in response to H19 depletion the let-7 targets were downregulated at both RNA (Figure 3A, second and third columns, compare red bars to blue bars) and protein (Figure 3B, compare lanes 2 to lanes 1 on the left, and red bars to blue bars on the right) levels. Importantly, in myotubes transfected with siCon, insulin stimulated glucose uptake by ∼2-fold (Figure 3C, left column, compare red bar to green bar). In contrast, there was no insulin-dependent stimulation of glucose uptake in myotubes transfected with simH19 (Figure 3C, right column, compare red bar to green bar). Consistent with an impaired insulin-PI3K-mTOR signaling, there was decrease in phosphorylation of both Akt and S6 in simH19-transfected versus siCon-transfected myotubes (Figure 3D, compare lane 3 to 1 in top and middle blots, respectively). Combining our *in vivo* (Figure 1) with *in vitro* (Figures 2 and 3) results, we suggest that decreased H19 in diabetic muscle cells may cause increased bioavailability of let-7, which in turn suppresses

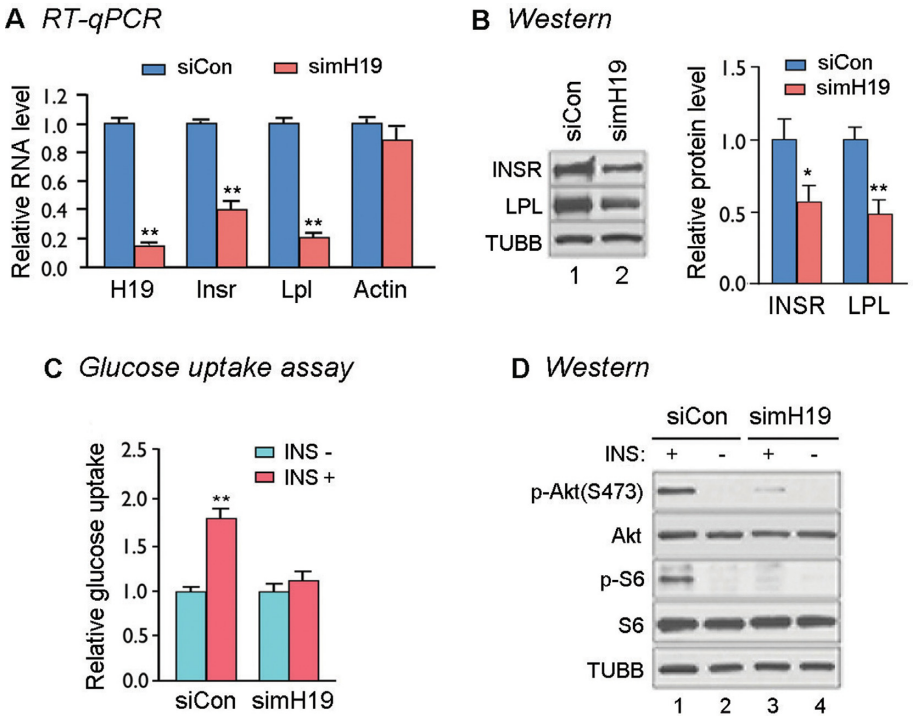

Figure 3. H19 regulates glucose uptake by affecting the insulin-PI3K-mTOR pathway. C3H myotubes were transfected with siCon or simH19. RNA and proteins were extracted and analyzed by RT-qPCR (**A**) and western blot (**B**) 48 h post transfection. Numbers are mean ± SEM ($n = 3$). *$P < 0.05$; **$P < 0.01$. (**C**) C3H myotubes were transfected with siCon or simH19. Glucose uptake was measured 48 h post-transfection. Results are presented as relative glucose uptake with values in absence of insulin stimulation set as 1. Numbers are mean ± SEM ($n = 6$). **$P < 0.01$. (**D**) Western blot analysis of effects of H19 knockdown on insulin-PI3K-mTOR signaling. C3H myotubes transfected with siCon or simH19 were insulin stimulated (+) or not stimulated (−) for 30 min. Proteins were extracted and analyzed using antibodies specific for the phosphorylated [p-Akt(S473)/p-S6] or total [Akt/S6] proteins known to be involved in the pathway. Beta-tubulin was used as loading controls.

expression of *Insr* and *Lpl*. We propose that H19 may contribute to muscle glucose regulation by acting as a novel upstream regulator of let-7.

Acute hyperinsulinemia downregulates H19 in non-diabetic muscle

A hallmark of T2D is decreased insulin-stimulated glucose uptake accompanied by compensatory hyperinsulinemia (a condition in which there are excess levels of insulin circulating in the blood) (36,37). While the cause of diminished H19 expression in T2D muscle is unknown, we observed H19 downregulation in muscle of non-diabetic rodents following acute hyperinsulinemia in hyperinsulinemic-euglycemic clamp studies. We used well-established conditions by the NIH-funded Mouse Metabolic Phenotyping Consortium in which both skeletal muscle insulin signaling and glucose transport are stimulated during the experiments (38).

Thus, following a 14 h overnight fast, healthy non-diabetic mice received a fixed infusion of insulin (3 mU/kg/min) and a variable infusion of 20% dextrose to maintain euglycemia for 140 min. In parallel, overnight fasted mice that had also undergone surgery were sacrificed for non-insulin stimulated tissue. Gastrocnemius and quadriceps muscle were isolated, followed by RNA extraction and RT-qPCR analysis. We observed an ∼80% decrease in H19 level at 140 min of hyperinsulinemia compared to the control (Figure 4A). Similar results were obtained from hyperinsulinemic-euglycemic clamp studies performed on non-diabetic rats (Supplementary Figure S5A). Our bioinformatic analyses predicted binding sites for six let-7 subtypes in rat H19 (12). In addition, HFD rats showed decreased levels of H19 in the skeletal muscle (Supplementary Figure S5B), as is the case for HFD mice (Figure 1A, right panel). Importantly, the hyperinsulinemia-induced H19 downregulation was recapitulated in C3H myotubes in which a high dose (100 nM) of insulin stimulation for 2 h led to H19 decrease by ∼60% (Figure 4B).

Regulation of H19 expression has been shown to occur mainly at the transcriptional level during mouse fetal development but at the post-transcriptional level during muscle cell differentiation (39). We thus asked whether the rapid H19 downregulation observed (Figure 4A and B) could be a result of H19 destabilization. H19 had a significantly faster decay rate in insulin stimulated versus un-stimulated myotubes (Figure 4C, left panel, compare red-dotted line with blue-dotted line), whereas no decay rate differences were observed with gapdh mRNA (right panel), suggesting that insulin-stimulated H19 downregulation occurs at least in part through RNA destabilization.

Downregulation of H19 is mediated by let-7

We noted previously that let-7 overexpression causes H19 level decline in let-7-transfected myotubes (12). We also noted that let-7 interacts with H19 in Ago2-containing

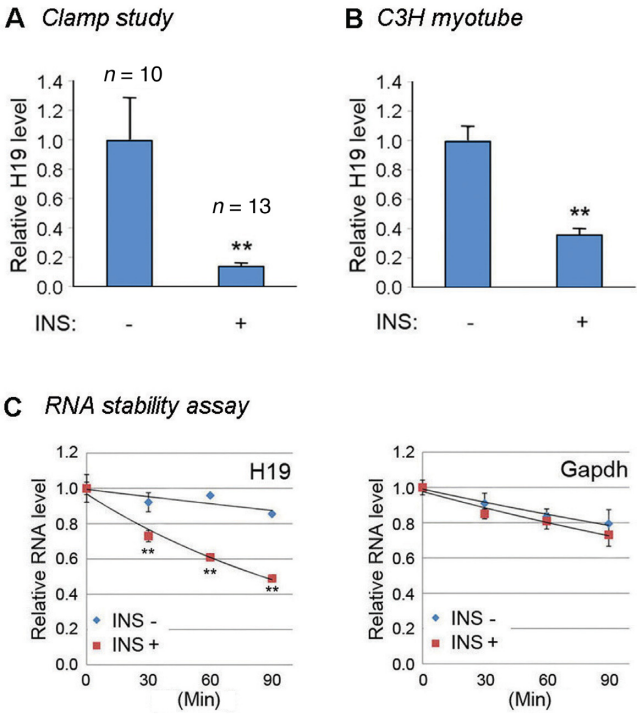

Figure 4. High dose insulin downregulates H19 both *in vivo* and *in vitro*. (**A**) H19 levels from skeletal muscle of non-diabetic mice subjected to clamp studies. INS+, with insulin infusion; INS−, without insulin infusion. Numbers are mean ± SEM. $^{**}P < 0.01$. (**B**) C3H myotubes were stimulated (INS+) or un-stimulated (INS−) with 100 nM of insulin for 2 h. RNAs were extracted and analyzed by RT-qPCR. Numbers are mean ± SEM. ($n = 3$); $^{**}P < 0.01$. (**C**) C3H myotubes were stimulated or un-stimulated by 100 nM of insulin in the presence of transcription inhibitor actinomycin D at a final concentration of 10 μg/ml. RNAs were collected at the indicated time points and levels determined by RT-qPCR. Results are presented after normalization against beta-tubulin mRNA, with zero time point mRNA levels arbitrarily set as 1. Numbers are mean ± SEM. ($n = 3$); $^{**}P < 0.01$.

RNPs (12). To test the possibility that binding of let-7 to H19 might induce H19 degradation, we transfected let-7 or miCon (control miRNA) into C3H myotubes, followed by RNA stability analysis. The decay rate of H19 was increased in cells transfected with let-7 compared to control miRNA (Supplementary Figure S6), consistent with let-7-mediated H19 destabilization. These observations prompted us to ask whether acute high dose insulin stimulation might increase let-7 levels, thereby promoting H19 destabilization. Thus, C3H myotubes were stimulated with 100 nM of insulin for 2 h and expression of let-7 was analyzed. The level of let-7 increased by ∼3-fold in response to insulin stimulation (Figure 5A), consistent with the notion that increased let-7 has a causative effect on H19 destabilization. Further, transfecting let-7 into myotubes resulted in decreased H19 expression (Figure 5B, compare middle column with left column), while transfecting miR-16 (predicted not to bind H19 (12)) did not (Figure 5B, left column). Thus, under our experimental conditions H19 destabilization appeared to be let-7-specific, although other mechanisms of action could not be ruled out.

To provide further evidence to support a let-7-specific effect, myotubes were transfected with iCon, iLet7 or imiR-16 (miR-16-specific inhibitor). Following overnight incubation, transfected cells were treated with or without 100 nM of insulin for 2 h. RNAs were extracted and analyzed by RT-qPCR. Both iCon- and imiR-16-transfected cells showed a decrease in the H19 level in response to insulin (Figure 5C, first two columns from left, compare red bars to blue bars). However, the decrease in H19 level no longer occurred with insulin in iLet7-transfected cells (right column, compare red bar with blue bar). Taken together these results led us to speculate that in C3H myotubes, high dose insulin upregulates let-7, which in turn downregulates H19. As hyperinsulinemia downregulates H19 in rodent skeletal muscle (Figure 4A and Supplemental Figure S5A), we predicted that hyperinsulinemia would upregulate let-7 in muscle, which indeed was the case. As demonstrated from our hyperinsulinemic-euglycemic clamp studies performed on non-diabetic mice, a high dose insulin perfusion for 140 min led to a ∼2.5-fold increase in the mature let-7 level (Figure 5D), suggesting that increased let-7 production likely contributes to H19 downregulation *in vivo*.

Let-7 upregulation requires KSRP and involves insulin/PI3K/AKT signaling

What could be the underlying mechanism of let-7 upregulation? It was recently reported that treating C3H myotubes with a high dose of insulin (100 nM) caused increased production of mature myogenic miRNAs, miR-1 and miR-133, as a result of enhanced processing of their primary transcripts (pri-miRNAs) (26). This enhanced processing required the RNA-binding protein KSRP, which was phosphorylated upon PI3K/AKT activation by insulin (26). Phosphorylation of KSRP by AKT enhanced KSRP's ability to interact with the myogenic pri-miRNAs and their processing into mature forms (26). This KSRP-dependent, insulin/PI3K/AKT-induced upregulation of miR-1 and miR-133 was recapitulated under our experimental conditions. Thus, we inhibited PI3K/AKT signaling in C3H myotubes using inhibitors shown to specifically inhibit the respective kinases at the indicated dosages (40–42), followed by examination of effects on expression of miR-1 and miR-133. The levels of mature miR-1 and miR-133 increased following 2 h insulin stimulation (Figure 6A, compare the second to the first bar from left), and were partially restored to those of non-insulin stimulated in the presence of either inhibitor (Figure 6A, compare third and fourth bars to the first). Further, when KSRP was silenced using a well-characterized siRNA specific for mouse KSRP (siKSRP) (26–28) (Supplementary Figure S7), the insulin-induced upregulation of both miRNAs was abolished (Figure 6B, compare right columns with the left). Together, our results are consistent with previous reports demonstrating that high dose insulin stimulation promotes biogenesis of miR-1 and miR-133 via a KSRP- and PI3K/AKT-dependent mechanism (26).

Given that KSRP also promotes processing of other pri-miRNAs including that of let-7 (27,43,44), we asked whether insulin-induced let-7 upregulation requires KSRP and whether it involves PI3K/AKT signaling. As expected, insulin induced an increase in mature let-7 by ∼2.5-fold in siCon-transfected C3H myotubes (Figure 6C, upper panel,

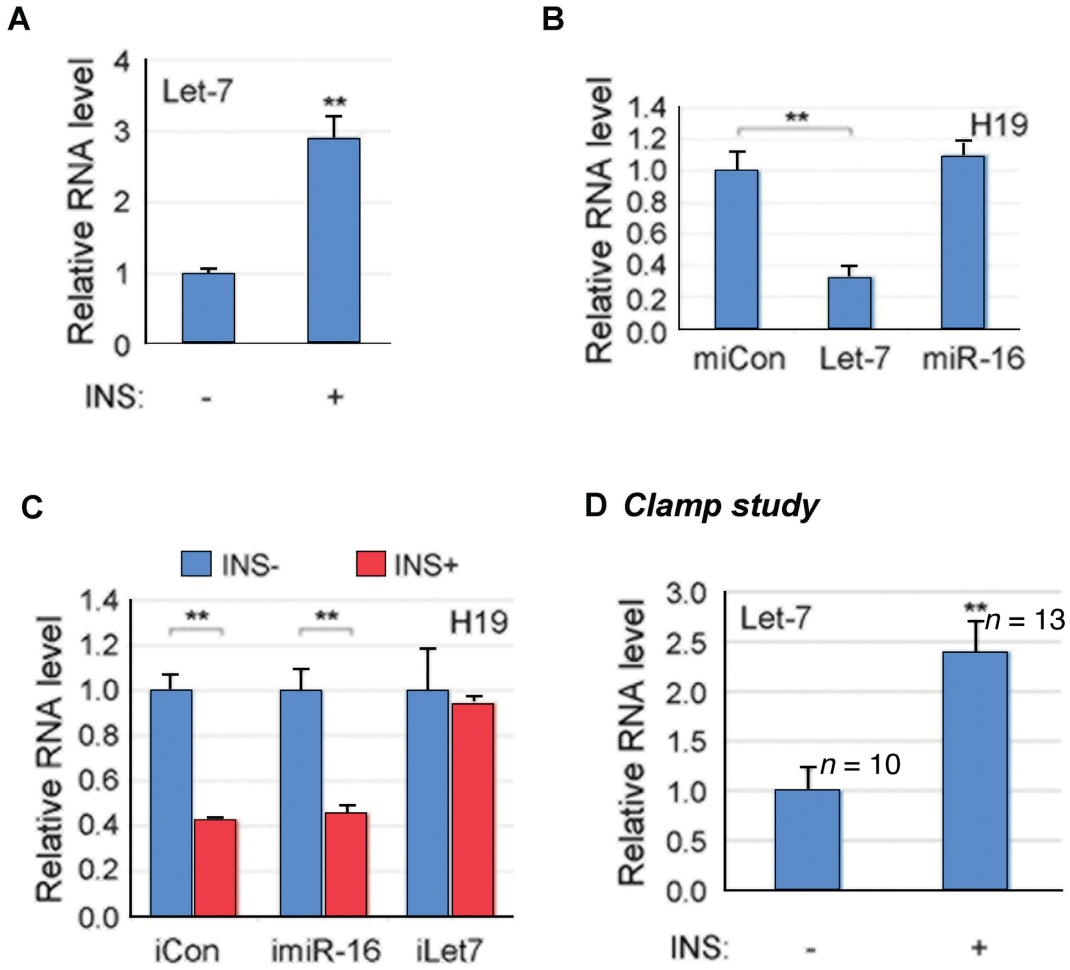

Figure 5. Insulin upregulates let-7 both *in vitro* and *in vivo*. (**A**) C3H myotubes were stimulated or un-stimulated with 100 nM of insulin for 2 h, followed by RNA extraction and RT-qPCR analysis. Relative levels of let-7 are shown. (**B**) C3H myotubes were transfected with control miRNA (miCon), let-7, or miR-16. RNAs were extracted 4 h later and RT-qPCR analysis performed. Relative H19 levels are presented with that of miCon-transfected arbitrarily set as 1. (**C**) C3H myotubes were transfected with iCon, imiR-16, or iLet7. After overnight incubation, transfected cells were stimulated or un-stimulated with 100 nM of insulin for 2 h. RNAs were extracted and analyzed by RT-qPCR. (**D**) Let-7 levels from skeletal muscle of non-diabetic mice subjected to clamp studies. All data are presented as mean ± SEM. ($n = 3$ when not indicated); $^{**}P < 0.01$.

left column, compare red bar to blue bar). This insulin-dependent increase was abrogated when KSRP was downregulated (right column), consistent with a requirement for KSRP for insulin-induced upregulation of let-7. Also as expected, the level of H19 decreased when let-7 was upregulated in siCon- but not in siKSRP-transfected myotubes (Figure 6C, bottom panel), further supporting the role of let-7 in mediating H19 destabilization.

To address whether activation of PI3K/AKT signaling plays a role in insulin-induced let-7 upregulation and H19 downregulation, C3H myotubes were treated with 100 nM of insulin for 2 h in the presence or absence of kinase inhibitors, followed by RT-qPCR analysis. While insulin increased let-7 levels (Figure 6D, compare the second to the first bar from left), co-incubation with either inhibitor abolished this insulin-dependent effect (compare the third and fourth bars to the second and first bars). Importantly, response of H19 to these inhibitors was consistent with let-7′s role as a negative regulator of its stability (Figure 6D, bottom panel). Taken together, these results strongly support a model in which KSRP and its PI3K/AKT-dependent activation play a role in the insulin-induced let-7 upregulation, which mediates H19 destabilization following acute hyperinsulinemia in non-diabetic muscle.

Insulin signaling remains intact during acute hyperinsulinemia in non-diabetic muscle

Following 100 nM of insulin stimulation of myotubes for 2 h (acute phase), the level of H19 decreased, as did the mRNA levels of Lpl and Insr (Figure 6E, top panel, compare red bars to blue bars). The level of H19 returned to normal at 24 h (later time point) following a single dose of insulin, although those of Lpl and Insr remained low (Figure 6E, bottom panel). Western blot analysis confirmed decreased protein levels of Lpl and Insr at 24 h post insulin stimulation (compare lane 2 to lane 1 in the top two blots in Figure 6F; pink bars to blue bars in Figure 6G), but not at 2 h (data not shown), which was not surprising as the 2 h time frame would not be sufficient to detect protein level

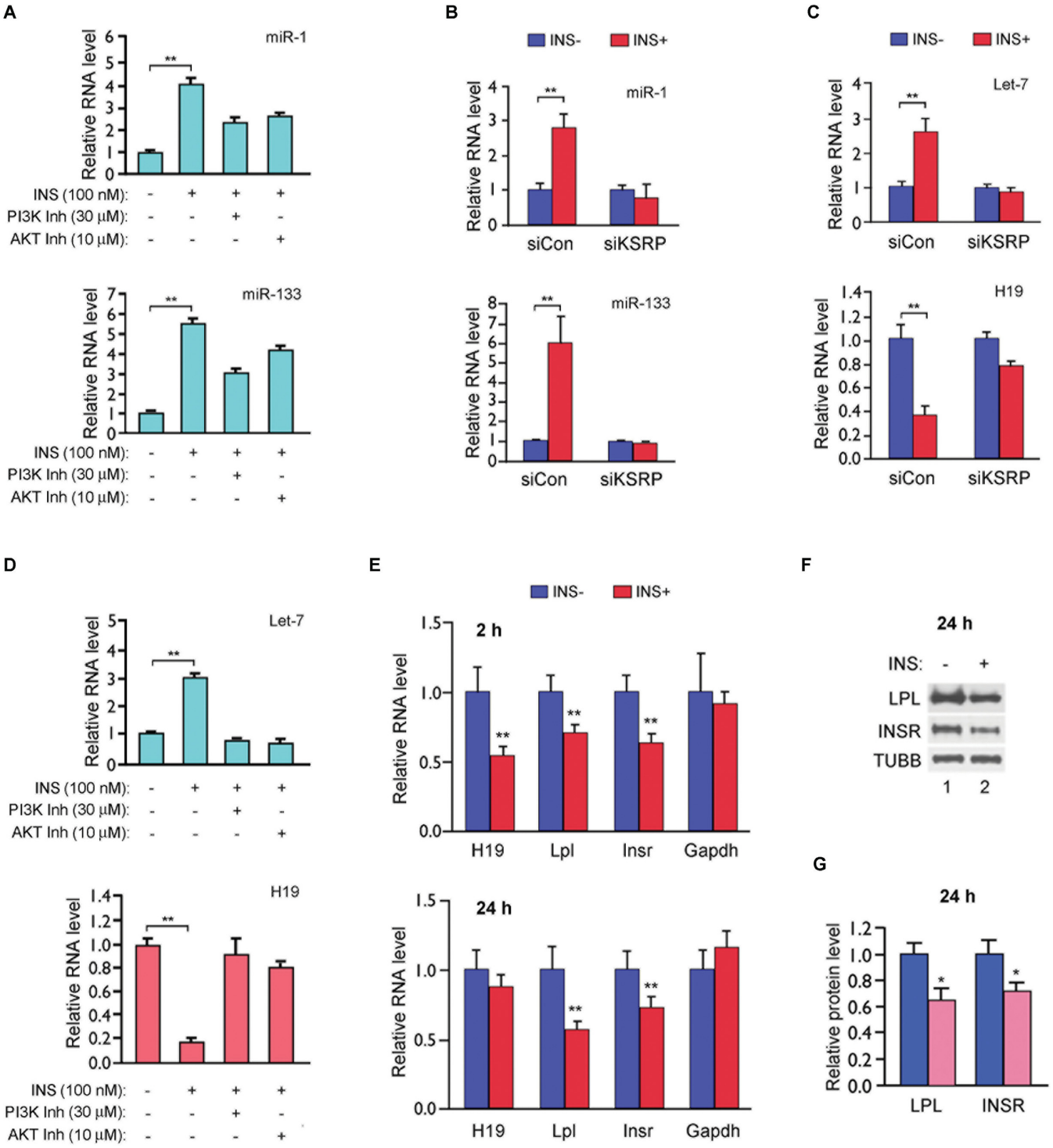

Figure 6. Let-7 upregulation requires KSRP and PI3K/AKT signaling. (**A**) C3H myotubes were stimulated (INS+) or un-stimulated (INS−) with 100 nM of insulin for 2 h, in the presence or absence of indicated kinase inhibitors. miRNAs were extracted and subjected to RT-qPCR analysis. Relative levels of mature miR-1 and miR-133 are shown on top and bottom panels, respectively. (**B** and **C**) C3H myotubes were transfected with siCon or siKSRP. Forty-eight hours later, cells were stimulated or un-stimulated with 100 nM of insulin for 2 h, following by RNA extraction and RT-qPCR analysis. (**D**) C3H myotubes were stimulated (INS+) or un-stimulated (INS−) with 100 nM of insulin for 2 h, in the presence or absence of indicated kinase inhibitors. RNAs were extraction and subjected to RT-qPCR analysis. Relative levels of let-7 and H19 are shown on top and bottom panels, respectively. All data are presented as mean ± SEM. ($n = 3$); $^{**}P < 0.01$. (**E**) C3H myotubes were stimulated (INS+) or un-stimulated (INS−) with 100 nM of insulin. RNAs were extraction at 2 h (top panel) or 24 h (bottom panel) and subjected to RT-qPCR analysis. Relative RNA levels are shown after normalization against beta-tubulin. Numbers are mean ± SEM. ($n = 3$); $^{**}P < 0.01$. (**F**) Proteins were extracted from C3H myotubes 24 h following stimulation with a single dose of 100 nM insulin (INS+) or no INS stimulation (INS−) and analyzed by western blot using antibodies against LPL (top blot), INSR (middle blot) and TUBB (bottom blot). (**G**) Quantification of western blot gels from three independent experiments. Numbers are presented as mean ± SEM. ($n = 3$); $^{**}P < 0.01$.

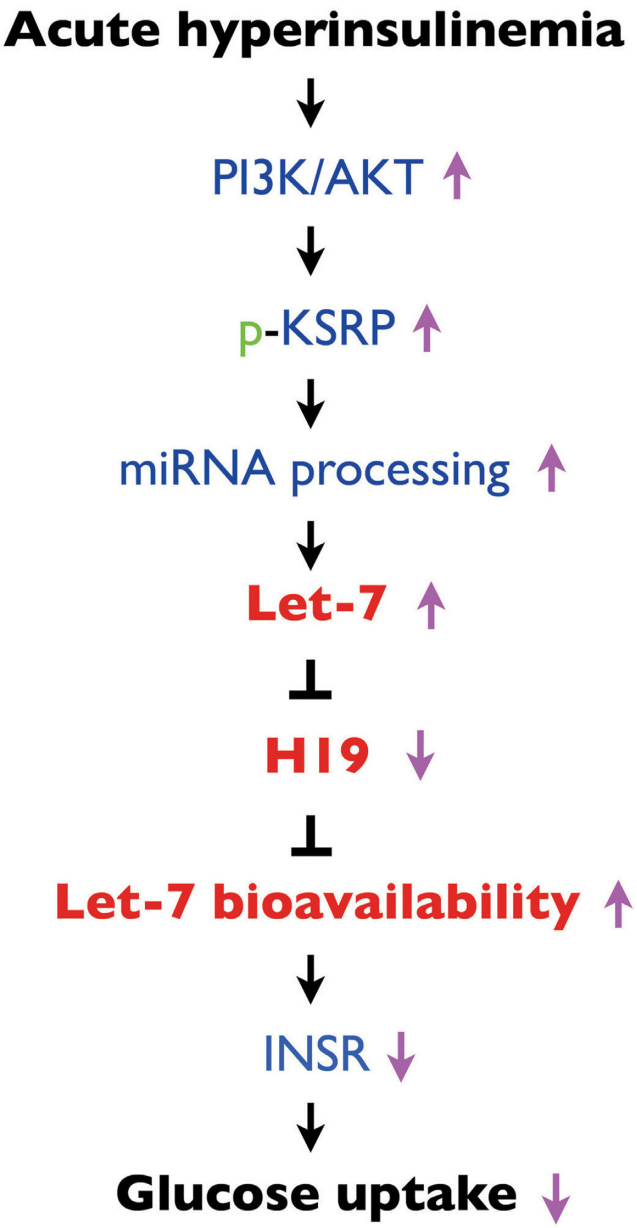

Figure 7. A proposed protective mechanism mediated by the H19/let-7 axis. Under normal conditions in non-diabetic muscle there exists a homeostasis with high H19 and low let-7 availability. During acute hyperinsulinemia, the PI3K/AKT pathway is activated, causing let-7 level rise and rapid H19 degradation. Such H19 depletion and release of let-7 leads to temporal impairment of insulin signaling at later time points, thus preventing muscle cells from overdrawing glucose from the circulation.

changes. Thus, insulin signaling would remain intact during acute phase but impaired at later time points when Insr and Lpl protein levels begin to fall. This would be consistent with the fact that hyperinsuinemia stimulates glucose uptake during acute phase in non-diabetic rodents (38) and that high dose insulin (100 nM) stimulates glucose uptake in siCon-transfected (but not simH19-transfected) C3H myotubes (Figure 3C).

DISCUSSION

Both our *in vivo* and *in vitro* studies suggest that H19 may regulate muscle glucose metabolism by acting as a novel upstream regulator of let-7 whose role in glucose metabolism has been firmly established (21,22). We provide evidence that in diabetic muscle decreased H19 leads to increased bioavailability of let-7, which in turn inhibits expression of key metabolic genes such as *Insr* and *Lpl*. On the other hand, let-7 targets H19 for degradation during acute hyperinsulinemia in non-diabetic muscle. Thus, there exists a double-negative feedback loop between H19 and let-7 that contributes to glucose regulation in muscle. Our results also help to explain, at least in part, the paradox phenomenon that HFD mice have impaired glucose metabolism but with a normal level of let-7 in their skeletal muscle (22).

Our finding that let-7 targets H19 for destabilization in response to extracellular cues establishes the first example of miRNAs regulating their own sponges as a part of a regulatory feedback loop. This regulation appears to serve as a protective mechanism in non-diabetic individuals. Results from both *in vivo* (Figures 4D and 5A) and *in vitro* (Figures 4A and 5B) studies demonstrate that acute high dose insulin stimulation increases let-7 and decreases H19, and that these effects are dependent on intact insulin signaling, as such effects are not observed in HFD muscle (Supplementary Figure S8). This suggests that in healthy individuals the 'off-signal' for the H19/let-7 axis is the normal rise and fall of plasma insulin following regular meals. During acute hyperinsulinemia, the axis is activated and serves as a protective mechanism to prevent muscle from overusing circulatory glucose at later time points which otherwise would be toxic to the muscle (Figure 7). The axis corrects itself following acute high insulin assault, which is supported by results from C3H myotubes (Figure 6E–G).

Unfortunately, the available H19 deletion mouse models are not suitable for studying H19-mediated regulation of glucose metabolism due to complex regulatory circuitry involving the imprinted gene network that controls embryo growth and muscle development (1,7,45,46). Further, global and constitutive H19 knockout could induce developmentally compensatory mechanisms that confound data interpretations. Further studies using transgenic mouse models that allow muscle-specific and inducible expression of H19 shRNA will be necessary to firmly establish the *in vivo* role for H19 in glucose metabolism.

SUPPLEMENTARY DATA

Supplementary Data are available at NAR Online.

ACKNOWLEDGMENT

We thank Sabrina Diano for critical reading and revision of the manuscript, Lingeng Lu for predicting let-7-binding sites in the human and mouse *Lpl* genes, Chaochun Liu and Ye Ding for preparing Supplementary Figure S2A.

FUNDING

Albert McKern Scholar Award [R01 DK-40936 to Y.H., U24 DK-059635 to G.I.S., R01 HD072418 to G.G.C.]. Funding for open access charge: NIH [R01 HD072418].
Conflict of interest statement. None declared.

REFERENCES

1. Gabory,A., Jammes,H. and Dandolo,L. (2010) The H19 locus: role of an imprinted non-coding RNA in growth and development. *Bioessays*, **32**, 473–480.
2. Yoshimizu,T., Miroglio,A., Ripoche,M.A., Gabory,A., Vernucci,M., Riccio,A., Colnot,S., Godard,C., Terris,B., Jammes,H. *et al.* (2008) The H19 locus acts in vivo as a tumor suppressor. *Proc. Natl. Acad. Sci. U.S.A.*, **105**, 12417–12422.
3. Matouk,I., Raveh,E., Ohana,P., Lail,R.A., Gershtain,E., Gilon,M., De Groot,N., Czerniak,A. and Hochberg,A. (2013) The increasing complexity of the oncofetal h19 gene locus: functional dissection and therapeutic intervention. *Int. J. Mol. Sci.*, **14**, 4298–4316.
4. Luo,M., Li,Z., Wang,W., Zeng,Y., Liu,Z. and Qiu,J. (2013) Long non-coding RNA H19 increases bladder cancer metastasis by associating with EZH2 and inhibiting E-cadherin expression. *Cancer Lett.*, **333**, 213–221.
5. Yan,L., Zhou,J., Gao,Y., Ghazal,S., Lu,L., Bellone,S., Yang,Y., Liu,N., Zhao,X., Santin,A.D. *et al.* (2014) Regulation of tumor cell migration and invasion by the H19/let-7 axis is antagonized by metformin-induced DNA methylation. *Oncogene*, doi:10.1038/onc.2014.236.
6. Ma,C., Nong,K., Zhu,H., Wang,W., Huang,X., Yuan,Z. and Ai,K. (2014) H19 promotes pancreatic cancer metastasis by derepressing let-7′s suppression on its target HMGA2-mediated EMT. *Tumour Biol.*, **35**, 9163–9169.
7. Monnier,P., Martinet,C., Pontis,J., Stancheva,I., Ait-Si-Ali,S. and Dandolo,L. (2014) H19 lncRNA controls gene expression of the Imprinted Gene Network by recruiting MBD1. *Proc. Natl. Acad. Sci. U.S.A.*, **110**, 20693–20698.
8. Cai,X. and Cullen,B.R. (2007) The imprinted H19 noncoding RNA is a primary microRNA precursor. *RNA*, **13**, 313–316.
9. Keniry,A., Oxley,D., Monnier,P., Kyba,M., Dandolo,L., Smits,G. and Reik,W. (2012) The H19 lincRNA is a developmental reservoir of miR-675 that suppresses growth and Igf1r. *Nat. Cell Biol.*, **14**, 659–665.
10. Venkatraman,A., He,X.C., Thorvaldsen,J.L., Sugimura,R., Perry,J.M., Tao,F., Zhao,M., Christenson,M.K., Sanchez,R., Yu,J.Y. *et al.* (2013) Maternal imprinting at the H19-Igf2 locus maintains adult haematopoietic stem cell quiescence. *Nature*, **500**, 345–349.
11. Dey,B.K., Pfeifer,K. and Dutta,A. (2014) The H19 long noncoding RNA gives rise to microRNAs miR-675–3p and miR-675–5p to promote skeletal muscle differentiation and regeneration. *Genes Dev.*, **28**, 491–501.
12. Kallen,A.N., Zhou,X.B., Xu,J., Qiao,C., Ma,J., Yan,L., Lu,L., Liu,C., Yi,J.S., Zhang,H. *et al.* (2013) The imprinted H19 lncRNA antagonizes let-7 microRNAs. *Mol. Cell*, **52**, 101–112.
13. Wang,J., Liu,X., Wu,H., Ni,P., Gu,Z., Qiao,Y., Chen,N., Sun,F. and Fan,Q. (2010) CREB up-regulates long non-coding RNA, HULC expression through interaction with microRNA-372 in liver cancer. *Nucleic Acids Res.*, **38**, 5366–5383.
14. Franco-Zorrilla,J.M., Valli,A., Todesco,M., Mateos,I., Puga,M.I., Rubio-Somoza,I., Leyva,A., Weigel,D., Garcia,J.A. and Paz-Ares,J. (2007) Target mimicry provides a new mechanism for regulation of microRNA activity. *Nat. Genet.*, **39**, 1033–1037.
15. Cazalla,D., Yario,T. and Steitz,J.A. (2010) Down-regulation of a host microRNA by a Herpesvirus saimiri noncoding RNA. *Science*, **328**, 1563–1566.
16. Poliseno,L., Salmena,L., Zhang,J., Carver,B., Haveman,W.J. and Pandolfi,P.P. (2010) A coding-independent function of gene and pseudogene mRNAs regulates tumour biology. *Nature*, **465**, 1033–1038.
17. Tay,Y., Kats,L., Salmena,L., Weiss,D., Tan,S.M., Ala,U., Karreth,F., Poliseno,L., Provero,P., Di Cunto,F. *et al.* (2011) Coding-independent regulation of the tumor suppressor PTEN by competing endogenous mRNAs. *Cell*, **147**, 344–357.
18. Cesana,M., Cacchiarelli,D., Legnini,I., Santini,T., Sthandier,O., Chinappi,M., Tramontano,A. and Bozzoni,I. (2011) A long noncoding RNA controls muscle differentiation by functioning as a competing endogenous RNA. *Cell*, **147**, 358–369.
19. Memczak,S., Jens,M., Elefsinioti,A., Torti,F., Krueger,J., Rybak,A., Maier,L., Mackowiak,S.D., Gregersen,L.H., Munschauer,M. *et al.* (2013) Circular RNAs are a large class of animal RNAs with regulatory potency. *Nature*, **495**, 333–338.
20. Hansen,T.B., Jensen,T.I., Clausen,B.H., Bramsen,J.B., Finsen,B., Damgaard,C.K. and Kjems,J. (2013) Natural RNA circles function as efficient microRNA sponges. *Nature*, **495**, 384–388.
21. Zhu,H., Shyh-Chang,N., Segre,A.V., Shinoda,G., Shah,S.P., Einhorn,W.S., Takeuchi,A., Engreitz,J.M., Hagan,J.P., Kharas,M.G. *et al.* (2011) The Lin28/let-7 axis regulates glucose metabolism. *Cell*, **147**, 81–94.
22. Frost,R.J. and Olson,E.N. (2011) Control of glucose homeostasis and insulin sensitivity by the Let-7 family of microRNAs. *Proc. Natl. Acad. Sci. U.S.A.*, **108**, 21075–21080.
23. Shyh-Chang,N. and Daley,G.Q. (2013) Lin28: primal regulator of growth and metabolism in stem cells. *Cell Stem Cell*, **12**, 395–406.
24. Thornton,J.E. and Gregory,R.I. (2012) How does Lin28 let-7 control development and disease? *Trends Cell Biol*, **22**, 474–482.
25. Huang,Y. (2012) A mirror of two faces: Lin28 as a master regulator of both miRNA and mRNA. *Wiley Interdiscip. Rev. RNA*, **3**, 483–494.
26. Briata,P., Lin,W.J., Giovarelli,M., Pasero,M., Chou,C.F., Trabucchi,M., Rosenfeld,M.G., Chen,C.Y. and Gherzi,R. (2012) PI3K/AKT signaling determines a dynamic switch between distinct KSRP functions favoring skeletal myogenesis. *Cell Death Differ.*, **19**, 478–487.
27. Trabucchi,M., Briata,P., Garcia-Mayoral,M., Haase,A.D., Filipowicz,W., Ramos,A., Gherzi,R. and Rosenfeld,M.G. (2009) The RNA-binding protein KSRP promotes the biogenesis of a subset of microRNAs. *Nature*, **459**, 1010–1014.
28. Briata,P., Forcales,S.V., Ponassi,M., Corte,G., Chen,C.-Y., Karin,M., Puri,P.L. and Gherzi,R. (2005) p38-dependent phosphorylation of the mRNA decay-promoting factor KSRP controls the stability of select myogenic transcripts. *Mol. Cell*, **20**, 891–903.
29. Onyango,P. and Feinberg,A.P. (2011) A nucleolar protein, H19 opposite tumor suppressor (HOTS), is a tumor growth inhibitor encoded by a human imprinted H19 antisense transcript. *Proc. Natl. Acad. Sci. U.S.A.*, **108**, 16759–16764.
30. Bruning,J.C., Michael,M.D., Winnay,J.N., Hayashi,T., Horsch,D., Accili,D., Goodyear,L.J. and Kahn,C.R. (1998) A muscle-specific insulin receptor knockout exhibits features of the metabolic syndrome of NIDDM without altering glucose tolerance. *Mol. Cell*, **2**, 559–569.
31. Mead,J.R., Irvine,S.A. and Ramji,D.P. (2002) Lipoprotein lipase: structure, function, regulation, and role in disease. *J. Mol. Med.*, **80**, 753–769.
32. Morino,K., Petersen,K.F., Sono,S., Choi,C.S., Samuel,V.T., Lin,A., Gallo,A., Zhao,H., Kashiwagi,A., Goldberg,I.J. *et al.* (2012) Regulation of mitochondrial biogenesis by lipoprotein lipase in muscle of insulin-resistant offspring of parents with type 2 diabetes. *Diabetes*, **61**, 877–887.
33. Morino,K., Petersen,K.F., Dufour,S., Befroy,D., Frattini,J., Shatzkes,N., Neschen,S., White,M.F., Bilz,S., Sono,S. *et al.* (2005) Reduced mitochondrial density and increased IRS-1 serine phosphorylation in muscle of insulin-resistant offspring of type 2 diabetic parents. *J. Clin. Invest.*, **115**, 3587–3593.
34. Befroy,D.E., Petersen,K.F., Dufour,S., Mason,G.F., de Graaf,R.A., Rothman,D.L. and Shulman,G.I. (2007) Impaired mitochondrial substrate oxidation in muscle of insulin-resistant offspring of type 2 diabetic patients. *Diabetes*, **56**, 1376–1381.
35. Petersen,K.F., Dufour,S., Befroy,D., Garcia,R. and Shulman,G.I. (2004) Impaired mitochondrial activity in the insulin-resistant offspring of patients with type 2 diabetes. *N. Engl. J. Med.*, **350**, 664–671.
36. Petersen,K.F., Dufour,S., Morino,K., Yoo,P.S., Cline,G.W. and Shulman,G.I. (2012) Reversal of muscle insulin resistance by weight reduction in young, lean, insulin-resistant offspring of parents with type 2 diabetes. *Proc. Natl. Acad. Sci. U.S.A.*, **109**, 8236–8240.
37. Warram,J.H., Martin,B.C., Krolewski,A.S., Soeldner,J.S. and Kahn,C.R. (1990) Slow glucose removal rate and hyperinsulinemia precede the development of type II diabetes in the offspring of diabetic parents. *Ann. Intern. Med.*, **113**, 909–915.

38. Ayala,J.E., Samuel,V.T., Morton,G.J., Obici,S., Croniger,C.M., Shulman,G.I., Wasserman,D.H., McGuinness,O.P. and Consortium,N.M.M.P.C. (2010) Standard operating procedures for describing and performing metabolic tests of glucose homeostasis in mice. *Dis. Model Mech.*, **3**, 525–534.
39. Milligan,L., Antoine,E., Bisbal,C., Weber,M., Brunel,C., Forne,T. and Cathala,G. (2000) H19 gene expression is up-regulated exclusively by stabilization of the RNA during muscle cell differentiation. *Oncogene*, **19**, 5810–5816.
40. Fransson,S., Uv,A., Eriksson,H., Andersson,M.K., Wettergren,Y., Bergo,M. and Ejeskar,K. (2012) p37delta is a new isoform of PI3K p110delta that increases cell proliferation and is overexpressed in tumors. *Oncogene*, **31**, 3277–3286.
41. Kim,K., Kim,K.H., Kim,H.Y., Cho,H.K., Sakamoto,N. and Cheong,J. (2010) Curcumin inhibits hepatitis C virus replication via suppressing the Akt-SREBP-1 pathway. *FEBS Lett.*, **584**, 707–712.
42. Boaglio,A.C., Zucchetti,A.E., Sanchez Pozzi,E.J., Pellegrino,J.M., Ochoa,J.E., Mottino,A.D., Vore,M., Crocenzi,F.A. and Roma,M.G. (2010) Phosphoinositide 3-kinase/protein kinase B signaling pathway is involved in estradiol 17beta-D-glucuronide-induced cholestasis: complementarity with classical protein kinase C. *Hepatology*, **52**, 1465–1476.
43. Nicastro,G., Garcia-Mayoral,M.F., Hollingworth,D., Kelly,G., Martin,S.R., Briata,P., Gherzi,R. and Ramos,A. (2012) Noncanonical G recognition mediates KSRP regulation of let-7 biogenesis. *Nat. Struct. Mol. Biol.*, **19**, 1282–1286.
44. Michlewski,G. and Caceres,J.F. (2010) Antagonistic role of hnRNP A1 and KSRP in the regulation of let-7a biogenesis. *Nat. Struct. Mol. Biol.*, **17**, 1011–1018.
45. Gabory,A., Ripoche,M.A., Le Digarcher,A., Watrin,F., Ziyyat,A., Forne,T., Jammes,H., Ainscough,J.F., Surani,M.A., Journot,L. *et al.* (2009) H19 acts as a trans regulator of the imprinted gene network controlling growth in mice. *Development*, **136**, 3413–3421.
46. Borensztein,M., Monnier,P., Court,F., Louault,Y., Ripoche,M.A., Tiret,L., Yao,Z., Tapscott,S.J., Forne,T., Montarras,D. *et al.* (2013) Myod and H19-Igf2 locus interactions are required for diaphragm formation in the mouse. *Development*, **140**, 1231–1239.